Exploring the binding kinetics of intracellular allosteric antagonists for CC chemokine receptor 2: a key to improve insurmountable antagonism

Yao, Y.; Hollander, L.S. den; Bleijs, B.; Hartung, T.; Grether, U.; Ortiz Zacarías, N.V.; Heitman, L.H.

Biochemical Pharmacology 249 (2026) 117864

Contents lists available at ScienceDirect

Biochemical Pharmacology

journal homepage: www.elsevier.com/locate/biochempharm

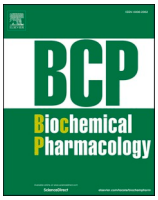

Exploring the binding kinetics of intracellular allosteric antagonists for CC chemokine receptor 2 — a key to improve insurmountable antagonism

Yao Yao [a], Lisa S. den Hollander [a], Bente Bleijs [a], Thomas Hartung [c], Uwe Grether [c], Natalia V. Ortiz Zacarías [a,b], Laura H. Heitman [a,b,*]

[a] Division of Medicinal Chemistry, Leiden Academic Centre for Drug Research, Leiden University, the Netherlands
[b] Oncode Institute, Leiden, the Netherlands
[c] Roche Pharma Research & Early Development, Roche Innovation Center Basel, F. Hoffmann-La Roche Ltd., Basel, Switzerland

ARTICLE INFO

Keywords:
CCR2
Binding kinetics
Residence time
Insurmountability
Competition association assay
Intracellular allosteric antagonists

ABSTRACT

CC chemokine receptor 2 (CCR2), a class A G protein-coupled receptor (GPCR), represents a promising therapeutic target for inflammatory and autoimmune diseases. Although several CCR2 antagonists have advanced to clinical trials, none have reached the market, largely due to limited efficacy. In recent decades, binding kinetics has emerged as a key consideration in early drug discovery, complementing traditional equilibrium parameters to enhance clinical efficacy. In parallel, targeting allosteric sites offers unique advantages, i.e. insurmountablility, further improving therapeutic safety and efficacy. However, the interplay between binding kinetics and allosterism has received little attention in drug discovery as a strategy to optimize insurmountablility.

As such, we developed a kinetic competition association assay, employing the intracellular allosteric radioligand [^{3}H]LUF7482, which displayed high affinity in both equilibrium and kinetic binding assays, with consistent nanomolar K_D values. After validation of the kinetic assay with unlabeled LUF7482, we profiled five known intracellular CCR2 antagonists, including the covalent binder LUF7834 as a positive control, which displayed an apparent long residence time (RT) of 576 min. Functional cAMP assays further revealed a strong correlation between binding kinetics and the extent of insurmountable antagonism.

Together, this study established the competition association assay as a robust approach to characterize the kinetic profiles of intracellular CCR2 antagonists, and revealed a clear correlation between binding kinetics and insurmountability. These findings may guide the selection and optimization of next-generation allosteric antagonists targeting CCR2, or the other GPCRs, in drug discovery pipelines, with the aim of improving insurmountability and, consequently, clinical efficacy.

1. Introduction

CC chemokine receptor 2 (CCR2) is a class A G protein-coupled receptor (GPCR) that primarily mediates the chemotaxis of monocytes [1] and macrophages [2] in response to its endogenous ligands, particularly CC chemokine ligand 2 (CCL2). The CCL2/CCR2 axis plays a critical role in immune cell recruitment and inflammatory responses [3], contributing to the pathogenesis of multiple diseases, including cancer [4], cardiovascular disorders [5], and autoimmune diseases [6]. Given its pivotal role in immune modulation and disease progression, CCR2 has been widely pursued as a promising therapeutic target, with numerous attempts to find effective therapies [7]. However, despite several

Abbreviations: $A_{2A}R$, adenosine A2A receptor; AUC, area under the curve; BCA, bicinchoninic acid; BSA, bovine serum albumin; B_{max}, maximum binding capacity; cAMP, cyclic adenosine monophosphate; CCL2, CC chemokine ligand 2; CCR2, CC chemokine receptor 2; CHAPS, 3-[(3-cholamidopropyl)-dimethyl ammonio]-1-propane sulfonate; DMSO, dimethyl sulfoxide; EC_{50}, half-maximal effective concentration; E_{max}, maximum response; ET, engagement time; GPCR, G protein-coupled receptor; $hENT_1$, human equilibrative nucleoside transporter 1; HPLC, high-performance liquid chromatography; IC_{50}, half-maximal inhibitory concentration; K_D, equilibrium dissociation constant; K_i, inhibition constant; k_{obs}, observed association rate constant; k_{off}, dissociation rate constant; k_{on}, association rate constant; $mGlu_2R$, metabotropic glutamate receptor 2; NanoBRET, NanoLuciferase bioluminescence resonance energy transfer; NSB, non-specific binding; PBS, phosphate buffered saline; RLU, relative light unit; RT, residence time; SEM, standard error of the mean; TB, total binding; TFA, trifluoroacetic acid; U2OS_hCCR2, Tango™ CCR2-*bla* U2OS; UV, ultraviolet.

* Corresponding author at: Division of Medicinal Chemistry, Leiden Academic Centre for Drug Research, Leiden University, the Netherlands.
E-mail address: l.h.heitman@lacdr.leidenuniv.nl (L.H. Heitman).

https://doi.org/10.1016/j.bcp.2026.117864
Received 19 December 2025; Received in revised form 26 February 2026; Accepted 27 February 2026
Available online 6 March 2026

candidates advancing into clinical trials, none have reached the market, largely due to limited efficacy [8].

Binding kinetics, a fundamental property of drug-receptor interactions, are increasingly recognized as critical determinants of drug efficacy, influencing both *in vivo* efficacy and duration of action [9,10]. In contrast to equilibrium binding parameters, which cannot capture the dynamics of drug-target interactions, kinetic parameters offer critical insights into how long and how fast a ligand engages its receptor [11]. Specifically, rapid association may promote early receptor occupancy and rebinding [12,13], while slow dissociation generally prolongs drug-target interactions and extends the biological effect [14]. Residence time (RT), defined as the reciprocal of dissociation rate constant (k_{off}), has emerged as a predictive *in vitro* parameter for *in vivo* efficacy, with studies demonstrating that compounds with long RT displayed better *in vivo* efficacy in animal models [10,15–17]. For targets involved in inflammatory diseases, i.e. chemokine receptors, high target occupancy (> 90%) is required to achieve effective inhibition [18]. Even minimal residual chemokine receptor activity can be sufficient to initiate positive feedback loops that drive inflammation [19]. Consequently, a long target RT is crucial to ensure sustained receptor occupancy and prolonged therapeutic action. Consistently, a long-RT CCR2 orthosteric antagonist (compound 15a in [20]), which achieved high receptor occupancy, was reported to effectively inhibit atherogenesis in an Apolipoprotein E deficient mouse model [20]. Taken together, an optimal balance of these kinetic properties can therefore improve *in vivo* efficacy, reduce dosing frequency, and enhance therapeutic outcomes.

While traditional strategies have focused on orthosteric antagonists that compete directly with endogenous agonists, intracellular allosteric antagonists have attracted increasing attention for their potential to achieve enhanced selectivity [21], and fine-tuned signaling modulation [22]. Moreover, unlike orthosteric inhibitors, which may be outcompeted by high concentrations of endogenous chemokines under pathophysiological conditions, intracellular allosteric antagonists engage alternative binding pockets that allow for insurmountable antagonism [23,24], whereby the allosteric antagonist suppresses the maximal agonist-induced response. Structural studies [25] and mutagenesis analysis [26] have demonstrated an intracellular binding site at CCR2 for small molecule antagonists, where pyrrolone [27], triazolopyrimidinone [23], and sulfonamide derivatives [28] have been reported to bind. Several of these antagonists, e.g. CCR2-RA-[*R*] [24] and LUF7721 (compound 39 in [23]), have been reported to display noncompetitive, insurmountable antagonism. Notably, the binding kinetics of intracellular allosteric CCR2 antagonists have previously been studied via NanoLuciferase bioluminescence resonance energy transfer (NanoBRET) assays with pyrrolone-based fluorescent ligands [29]. Nevertheless, the potential relationship between their binding kinetics and insurmountable behavior, are not yet fully understood.

To address this, we developed a competition association assay employing the allosteric radioligand [^{3}H]LUF7482, which allowed us to quantify the binding kinetics of several intracellular allosteric CCR2 antagonists. Considering that longer RT lead to more prolonged receptor occupancy and a higher likelihood of insurmountable antagonism, we hypothesized that RT correlates with functional insurmountability. To test this, three intracellular antagonists with diverse kinetic profiles were selected, and potential insurmountability was investigated using functional cyclic adenosine monophosphate (cAMP) assays. Applying this platform, we identified intracellular CCR2 antagonists with prolonged RTs, highlighting their potential to achieve favorable clinical efficacy. Given CCR2′s role in inflammatory diseases and cancer, intracellular allosteric antagonists with optimized kinetic profiles may provide a promising strategy for next-generation therapies with enhanced efficacy and safety.

2. Materials and METHODS

2.1. Chemicals and reagents

The human recombinant chemokine CCL2 was purchased from PeproTech (Rocky Hill, NJ, USA). Tango™ CCR2-*bla* U2OS (U2OS_hCCR2) cells was obtained from Invitrogen (Carlsbad, CA, USA). LUF6980 (SD-24), LUF7482, LUF7834, and LUF7521 were synthesized in-house as described previously [23,28,30]. JNJ-27141491 was purchased from Syncom B.V. (Groningen, The Netherlands), and CCR2-RA-[*R*] was purchased from Bio-Connect B.V. (Gelderland, The Netherlands).

Dimethyl sulfoxide (DMSO, anhydrous, ≥ 99.9%), phosphate buffered saline (PBS), and bovine serum albumin (BSA, Fraction V) were obtained from Sigma-Aldrich (Steinheim, Germany). McCoy's 5A medium was purchased from Thermo Fisher Scientific (Waltham, MA, USA). Non-essential amino acids and CO_2-independent medium were purchased from Gibco (Frederick, MD, USA). Hygromycin B gold and Zeocin™ were obtained from InvivoGen (San Diego, CA, USA). The Pierce™ bicinchoninic acid (BCA) protein assay kit and BSA standard ampules were purchased from Thermo Fisher Scientific (Waltham, MA, USA). The GloSensor™ cAMP assay kit was obtained from Promega (Madison, WI, USA). Forskolin was purchased from Toronto Research Chemicals Inc. (Toronto, ON, Canada).

Buffers and solutions were prepared at room temperature using Millipore water purified with a Milli-Q® EQ 7000 ultrapure water purification system (Sigma-Aldrich, Steinheim, Germany) and filtered through a 0.22 μm filter. Tris was obtained from SERVA Electrophoresis GmbH (Heidelberg, Germany); HCl (37% in water) from Acros (Geel, Belgium); $MgCl_2{\cdot}6H_2O$ from Sigma-Aldrich (Steinheim, Germany); and 3-[(3-cholamidopropyl)-dimethyl ammonio]-1-propane sulfonate (CHAPS, ≥ 98%) from Carl Roth GmbH & Co. KG (Karlsruhe, Germany).

All solvents for radioligand preparation were of analytical or high-performance liquid chromatography (HPLC) grade. Crabtree's catalyst [Ir(cod)(PCy_3)(py)]PF_6 was obtained from Sigma-Aldrich (Steinheim, Germany), dichloromethane (extra dry) was purchased from Thermo Scientific Chemicals (Waltham, MA, USA), acetonitrile was obtained from Biosolve (Dieuze, France), and trifluoroacetic acid, sodium bicarbonate, methanol, and ethanol were sourced from Merck KGaA (Darmstadt, Germany) and used as received. Carrier-free tritium gas was released from uranium tritide stored on a uranium bed of the tritium manifold system (RC Tritec AG, Teufen, Switzerland). All other chemicals and reagents were purchased from standard commercial sources.

2.2. Preparation of [^{3}H]LUF7482

[^{3}H]LUF7482 was custom-labeled by RC Tritec AG (Teufen, Switzerland) using an iridium-catalyzed H/T exchange reaction. In a micro-reaction vessel, 2.69 mg (5.69 μmol) of unlabeled LUF7482 and 14.4 mg (17.9 μmol) of Crabtree's catalyst were dissolved in 0.4 mL of dichloromethane. The mixture was frozen in liquid nitrogen, and the flask evacuated before closing the vacuum tap and being allowed to warm to room temperature. This procedure was performed three times. The mixture was frozen once more, and the flask was evacuated before 679 mbar of carrier-free tritium gas was released and directed into the reaction mixture. Upon equilibration, the pressure dropped to 477 mbar, corresponding to a calculated total system volume of 5.9 mL. Upon thawing to room temperature, the pressure increased to 743 mbar.

After stirring for 5 h at room temperature, the reaction was terminated. The solution was frozen with liquid nitrogen, leading to a pressure decrease to 361 mbar. Residual tritium gas was returned to the waste-gas storage bed, and the solvent was condensed into an ampoule. The residue was dissolved in 0.3 mL of methanol, followed by solvent removal by condensation. This procedure was performed three times. The resulting residue was suspended in 5 mL of ethanol and passed through a 0.2 μm syringe filter to yield the crude product.

For the subsequent preparative HPLC purification, the entire solution containing approximately 1 Ci (37 GBq) of crude product was concentrated to approximately 300 µL. Five portions of 50 µL each were injected on a Waters SunFire C18 column (10 × 250 mm, 5 µm; mobile phase: (A) H_2O + 0.1% trifluoroacetic acid (TFA); (B) acetonitrile + 0.1% TFA; isocratic elution: 31% A and 69% B; flow rate: 4.7 mL/min; ultraviolet (UV) detection at 254 nm. Fractions corresponding to the product peak (8.1–8.4 min) were collected, combined and neutralized with an equimolar amount of 10% aqueous $NaHCO_3$. The acetonitrile concentration was reduced by rotary evaporation at ≤ 45 °C. The tritiated radioligand was isolated from the remaining solution by solid-phase extraction using a Phenomenex Strata-X cartridge (3 mL, 100 mg) after washing it with water followed by elution with 5 mL of ethanol.

A total amount of 58.8 mCi (2.18 GBq) of [^{3}H]LUF7482 was obtained in a specific activity of 40.3 Ci/mmol (1.49 TBq/mmol), determined by mass spectrometry (Agilent 1290 high pressure gradient system and Agilent 6545 QTOF, flow 0.3 mL/min of 50% 0.02% formic acid in water and acetonitrile) and a radiochemical purity of > 98% determined by radio-HPLC (Waters SunFire C18, 4.6 × 250 mm, 5 µm; mobile phase: A: H_2O + 0.05% TFA, B: acetonitrile + 0.05% TFA, gradient elution 50–100% B over 10 min; 1 mL/min; 30 °C: UV at 254 nm plus flow-through radiomonitor).

2.3. Cell culture and membrane preparation

U2OS cells, which stably express human CCR2b (U2OS_hCCR2), were cultured at 37 °C, 5% CO_2, in McCoy's 5A medium supplemented with 10% (v/v) fetal calf serum, 2 mM glutamine, 0.1 mM non-essential amino acids, 25 mM HEPES, 1 mM sodium pyruvate, 200 IU/mL penicillin, 200 µg/mL streptomycin, 100 µg/mL G418, 40 µg/mL hygromycin B gold, and 125 µg/mL zeocin under a humidified atmosphere. U2OS_hCCR2 cells were cultured in 10 or 15 cm Ø plates until 80% confluence and sub-cultured twice weekly by trypsinization. Dialyzed fetal calf serum was used when culturing cells for functional assays or as the last step before membrane preparation.

For membrane preparation, cells were scraped into PBS and centrifuged for 5 min at 3000 rpm. The pellet was then resuspended in ice-cold buffer of 50 mM Tris-HCl (pH 7.4), supplemented with 5 mM $MgCl_2$ before homogenization with an Ultra Turrax homogenizer (IKA-Werke GmbH & Co. KG, Staufen, Germany). In two centrifugation steps using an Optima LE-80 K ultracentrifuge (Beckman Coulter, Inc., Fullerton, CA) at 31000 rpm for 20 min at 4 °C, the membrane fraction was separated. The resulting pellet was resuspended in ice-cold buffer of 50 mM Tris-HCl (pH 7.4), supplemented with 5 mM $MgCl_2$ and stored at −80 °C. Protein concentrations of membranes were determined using a standard Pierce™ BCA protein assay kit.

2.4. [^{3}H]LUF7482 displacement assay

Displacement assays with [^{3}H]LUF7482 were performed in a total reaction volume of 100 µL, containing 50 mM Tris-HCl (pH 7.4), 5 mM $MgCl_2$, 0,1% CHAPS, and 10–20 µg of U2OS_hCCR2 membranes at 15 °C. In the homologous displacement assay, ~1.5, ~6.5 and ~20 nM of [^{3}H]LUF7482 were competed with unlabeled LUF7482 at increasing six concentrations (10 pM – 1 µM). In the heterologous displacement assays, ~6.5 nM [^{3}H]LUF7482 was competed with five reference CCR2 antagonists at six increasing concentrations (0.1 nM – 10 µM). Total binding (TB) was determined by addition of vehicle (1% DMSO), while non-specific binding (NSB) was determined by addition of LUF7721 (10 µM). Note, DMSO concentrations were kept constant at 1% (v/v) in all samples.

Binding was initiated by the addition of membranes, and reaction mixtures were incubated for 120 min at 15 °C while shaking at 400 rpm. Ligand-receptor interaction was terminated by harvesting, which removed unbound radioligand using ice-cold washing buffer (50 mM Tris-HCl, pH 7.4; 5 mM $MgCl_2$; 0.05% CHAPS) on GF-C filters using a Filtermate harvester (Revvity, Groningen, The Netherlands). Radioactivity was measured through scintillation spectrometry using the P-E 2450 Microbeta^2 scintillation plate counter (Revvity, Groningen, The Netherlands) following the addition of 25 µL Microscint scintillation (Revvity, Groningen, The Netherlands).

2.5. [^{3}H]LUF7482 association and dissociation assays

[^{3}H]LUF7482 association assays were performed similarly to the displacement assay described in Section 2.4, in a total reaction volume of 100 µL containing ~6.5 nM [^{3}H]LUF7482 in the absence (vehicle) of competing compounds. Association of [^{3}H]LUF7482 was initiated by adding 20 µg U2OS_hCCR2 membranes at 11 different timepoints over a total incubation time of 120 min at 15 °C, while shaking at 400 rpm. [^{3}H]LUF7482 dissociation assays were carried out following a 120 min pre-incubation of ~6.5 nM [^{3}H]LUF7482 with 20 µg of U2OS_hCCR2 membranes to reach equilibrium at 15 °C, while shaking at 400 rpm. Subsequently, dissociation of the radioligand was initiated by adding a high concentration of displacer in a small volume (10 µM LUF7721 in 5 µL) at 11 different timepoints over a total incubation time of 120 min at 15 °C while shaking at 400 rpm. The amount of receptor-bound radioligand was determined after harvesting as described in Section 2.4 ('[^{3}H]LUF7482 Displacement Assay').

2.6. [^{3}H]LUF7482 competition association assay

The binding kinetics of unlabeled compounds were determined at 15 °C using a [^{3}H]LUF7482 competition association assay. Reactions were performed in a total reaction volume of 100 µL containing ~6.5 nM [^{3}H]LUF7482 in the absence (vehicle) or presence of competing compounds.

The assay was first validated using three concentrations of the unlabeled ('cold') ligand LUF7482: 12 nM (0.3× IC_{50}), 40 nM (1× IC_{50}) and 120 nM (3× IC_{50}). Binding kinetics of all other reference compounds were assessed using a simplified, one-concentration competition association assay [31]. Specifically, the radioligand was preincubated with either competing compounds (1× IC_{50}) or vehicle (1% DMSO) in assay buffer at 15 °C for 30 min while shaking at 400 rpm. Competition association assays were subsequently initiated by adding 20 µg of U2OS_hCCR2 membranes in assay buffer, at 11 time points over a 120 min incubation at 15 °C. Incubations were terminated by harvesting and the amount of receptor-bound radioligand was determined after harvesting as described in Section 2.4 ('[^{3}H]LUF7482 displacement assay').

2.7. GloSensor™ cAMP assay

The GloSensor™ cAMP assay (Promega, Madison, WI, USA) was performed according to the manufacturer's protocol. Briefly, U2OS_hCCR2 cells were seeded in 10 cm ø plates (2 × 10^6 cells/plate) for 24 h to reach ~50% confluence. Cells were then transfected with 10 µg of GloSensor™ cAMP plasmid, and grown until ~80% confluence for 24 h. Subsequently, transfected cells were seeded (50,000 cells/well) in a 96-well, white, flat-bottom plate (cat. no. 3917, Corning® Costar®, Cambridge, MA, USA) and incubated overnight. The next day, transfected cells were refreshed with 30 µL CO_2-independent medium, followed by addition of 50 µL/well of GloSensor™ cAMP reagent (final concentration of 2% reagent per well, diluted in CO_2-independent medium and prepared in the dark). The plate was mixed for 2 h at 25 °C, and in the dark, to allow luminescence to equilibrate. Baseline luminescence at 595 nm was monitored for 7.5 min with an EnVision multilabel plate reader (Revvity, Groningen, The Netherlands). Before antagonists addition, cells were stimulated with 1 µM forskolin for 52 min to induce cAMP production. Antagonists were prepared at the selected concentrations (30, 100, 300 nM) in CO_2-independent medium containing a 0.25% DMSO (final concentration). Cells were then

preincubated with each antagonist or the vehicle control (0.25% DMSO) for either 10 min or 120 min. Preincubated cells were subsequently stimulated with nine increasing concentrations of CCL2 (ranging from 10 pM to 0.3 μM). The final DMSO concentrations were kept at 0.25% in all wells. Directly after agonist stimulation, luminescence at 595 nm was measured for 90 min in real time.

2.8. Data analysis and statistics

All data were analyzed using GraphPad Prism 10.1 (GraphPad software, San Diego, CA, USA). Specific radioligand binding was calculated by subtracting non-specific binding (10 μM LUF7721). Data were subsequently normalized to total binding (vehicle control, 1% DMSO), set as 100%, except in homologous displacement experiments.

[^{3}H]LUF7482 homologous displacement data were analyzed using the 'One site – Homologous' model to obtain the equilibrium dissociation constant (K_D) and maximum binding capacity (B_{max}). Heterologous displacement data were analyzed using the 'One site – Fit logIC$_{50}$' model to determine IC$_{50}$ and pIC$_{50}$ values. The inhibition constant (K_i) was calculated using the 'One site – Fit K_i' function, according to the Cheng and Prusoff equation [32]:

$$K_i = \mathrm{IC}_{50} \Big/ \left(1 + \frac{[RL]}{K_D}\right)$$

where [RL] is the radioligand concentration (~6.5 nM, calculated from total counts), and K_D (10 nM) was obtained from [^{3}H]LUF7482 homologous displacement.

[^{3}H]LUF7482 association and dissociation data were fitted with 'one-phase association' or 'one-phase decay' to obtain the observed association (k_{obs}) and dissociation [k_{off} (k_2)] rate constants for [^{3}H]LUF7482, respectively. The association rate constant [k_{on} (k_1)] for [^{3}H]LUF7482 was calculated as follows:

$$k_{on} = (k_{obs} - k_{off})/[RL]$$

The kinetic dissociation rate constant (K_D) of the radioligand was then calculated as:

$$K_D = k_{off}/k_{on} = k_2/k_1$$

[^{3}H]LUF7482 competition association data were analyzed by fitting the data to the 'kinetics of competitive binding' model [33].

$$K_A = k_1\,[L] + k_2$$

$$K_B = k_3\,[I] + k_4$$

$$S = \sqrt{(K_A - K_B)^2 + 4\,k_1 k_3\,[L]\,[I]\,10^{-18}}$$

$$K_F = 0.5(K_A + K_B + S)$$

$$K_S = 0.5(K_A + K_B - S)$$

$$\mathrm{Q} = \frac{B_{max} k_1 [L] 10^{-9}}{K_F - K_S}$$

$$\mathrm{Y} = \mathrm{Q}\left(\frac{k_4(K_F - K_S)}{K_F K_S} + \frac{k_4 - K_F}{K_F} e^{(-K_F X)} - \frac{k_4 - K_S}{K_S} e^{(-K_S X)}\right)$$

In this model, X represents time (min), Y is the specific radioligand binding (DPM), and [I] is the concentration of unlabeled ligand (nM), Constraining these parameters, along with previously introduced k_{on} (k_1), k_{off} (k_2), [RL] and B_{max} allows the calculation of association [k_{on} (k_3)] and dissociation [k_{off} (k_4)] rate constants for competing compounds. All competition association data were globally fitted. The K_D values of competing compounds were calculated as:

$$K_D = k_{off}/k_{on} = k_4/k_3$$

Residence time (RT) was calculated as:

$$\mathrm{RT} = 1/k_{off}$$

To enable comparison and ranking of compounds, engagement time (ET) was calculated at a compound concentration of 1 μM. At this concentration, most compounds approach target saturation, providing a more robust and reliable kinetic readout. ET of compound at 1 μM was calculated as described previously [34]:

$$\mathrm{ET} = 1/(k_{on} \times 10^{-6})$$

GloSensor cAMP kinetic luminescence data were analyzed by calculating the area under the curve (AUC) over 90 min following CCL2 stimulation. AUC values were baseline-corrected using vehicle control, and normalized to the maximum response (E_{max}) of CCL2 (100%) in absence of antagonists. Data were then fitted to the non-linear regression function 'log (agonist or inhibitor) vs. response (three parameters)' to obtain EC$_{50}$ and E_{max} values.

All data were presented as mean ± standard error of the mean (SEM). Statistical differences between two experimental groups were evaluated using unpaired, two-tailed t-test with Welch's correction. Statistical differences among values for multiple individual groups were analyzed using Brown-Forsythe and Welch ANOVA followed by Dunnett's T3 multiple comparisons test: $p < 0.033$ was considered as statistical significant.

3. Results

3.1. Characterization of newly synthesized radioligand [^{3}H]LUF7482

A previous study introduced LUF7482 as a suitable candidate that binds the intracellular binding pocket of CCR2, and a radiolabeled analogue, [^{3}H]LUF7482, was subsequently synthesized [35]. To optimize the specific binding window of this radioligand to U2OS cells stably expressing human CCR2b (U2OS_hCCR2), we studied different buffer components, filter pre-treatment, membrane and radioligand concentrations (data not shown), resulting in the previously published assay [35].

The kinetic behavior of [^{3}H]LUF7482 on U2OS_hCCR2 was characterized using association (Fig. 1A) and dissociation assays (Fig. 1B), both of which displayed a monophasic kinetic profile of the radioligand. Since [^{3}H]LUF7482 exhibited rapid association and dissociation at 25 °C, accurate determination of kinetic parameters was only feasible at a reduced temperature of 15 °C. At this temperature, [^{3}H]LUF7482 displayed an association rate constant k_{on} of 3.3 × 10^7 M^{-1}·min^{-1} and a dissociation rate constant k_{off} of 0.12 min^{-1}. The corresponding kinetic dissociation constant (K_D), calculated from k_{on} and k_{off}, was 4 nM, with a residence time (RT) of 8.6 min (Table 1).

To further characterize its binding properties, homologous displacement assays were performed with increasing concentrations of unlabeled LUF7482 (ranging from 10 pM to 1 μM) to displace [^{3}H]LUF7482 at three radioligand concentrations (~1.5, 6.5, and 20 nM). These assays yielded a maximum binding capacity (B$_{max}$) of 6.3 pmol/mg protein and an equilibrium dissociation constant (K_D) of 10 nM (Fig. 1C, Table 1), consistent with the K_D value obtained from the kinetic studies.

3.2. [^{3}H]LUF7482 displacement by reference compounds

To determine the affinity of the selected reference antagonists, [^{3}H]LUF7482 displacement assays were performed. Six structurally diverse reference compounds were selected (structures shown in Fig. 2A), including three sulfonamide derivatives (LUF7834 [30], LUF7482, and

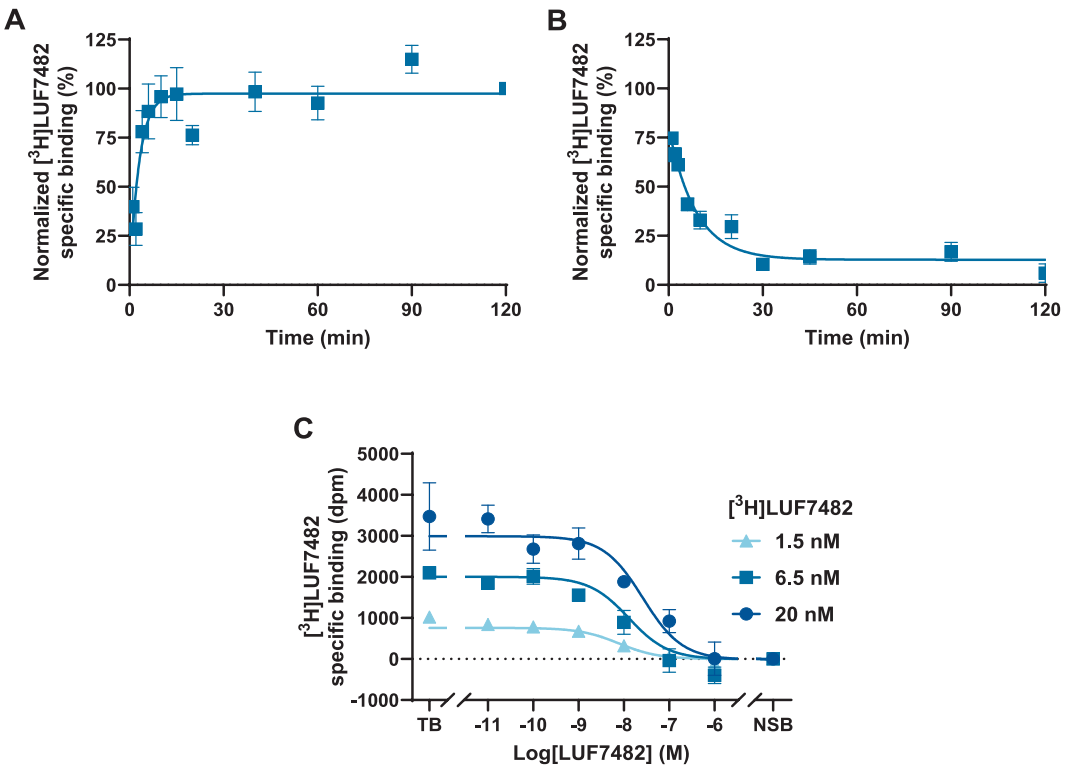

Fig. 1. Characterization of [^{3}H] LUF7482 binding kinetics on U2OS_hCCR2 membranes. (A, B) Association (A) and dissociation (B) of 6.5 nM [^{3}H]LUF7482 on U2OS_hCCR2 membranes over 120 min at 15 °C ($n = 4$). (C) Homologous displacement of [^{3}H]LUF7482 (~1.5, 6.5, and 20 nM) by non-labeled LUF7482 (10 pM – 1 μM) on U2OS_hCCR2 membranes at 15 °C ($n = 3$). Total binding (TB) was determined with vehicle control (1% DMSO), while non-specific binding (NSB) was determined in the presence of 10 μM LUF7721. Specific binding was calculated by subtracting NSB from total radioligand binding at each concentration and timepoint. Kinetic data were normalized to TB (100%) and NSB (0%). Parameters obtained from the association and dissociation curves (K_D, k_{on}, k_{off}, RT) and from the homologous displacement (B_{max}, K_D) are summarized in Table 1. Data are presented as the mean ± SEM of at least three independent experiments performed in duplicate.

Table 1
Characterization of [^{3}H] LUF7482 on U2OS_hCCR2 membranes at 15 °C.

Assay	B_{max} (pmol/mg)[a]	K_D (nM)	k_{on} (M^{-1}·min^{-1})[c]	k_{off} (min^{-1})[d]	RT (min)[e]
Association and Dissociation ($n = 4$)	–	4 ± 1[b]	(3.3 ± 0.4) × 10^7	0.12 ± 0.01	8.6 ± 1.1
Homologous Displacement ($n = 3$)	6.3 ± 0.9	10 ± 2[a]	–	–	–
Standard Competition Association ($n = 4$)	–	19 ± 6[b]	(2.1 ± 0.4) × 10^7	0.30 ± 0.05	3.4 ± 0.5

Values are presented as mean ± SEM from at least three independent experiments, each performed in duplicate. Statistical differences among multiple assays were analyzed using Brown-Forsythe and Welch ANOVA followed by Dunnett's T3 multiple comparisons test. No statistically significant differences were detected ($p > 0.033$).

[a] Maximum binding capacity (B_{max}) and equilibrium dissociation constant (K_D), derived from [^{3}H]LUF7482 homologous displacement assays on U2OS_hCCR2 membranes at 15 °C.

[b] Kinetic K_D values, calculated as $K_D = k_{off} / k_{on}$.

[c] Association rate constant (k_{on}) of [^{3}H]LUF7482 on U2OS_hCCR2 membranes at 15 °C.

[d] Dissociation rate constant (k_{off}) of [^{3}H]LUF7482 on U2OS_hCCR2 membranes at 15 °C.

[e] Residence time (RT), calculated as RT = 1 / k_{off}.

LUF6980 [28]), a triazolo-pyrimidinone (LUF7521 [23]), a 2-thioxoimidazoline (JNJ-27141491), and a pyrrolidinone (CCR2-RA-[R]). The sulfonamide LUF7834, which bears an acrylamide warhead, is known to bind irreversibly to CCR2 [30]. Therefore, it is expected to display a long residence time in binding kinetic assays as well as clear insurmountable antagonism in functional assays, making it a suitable 'positive control', to verify a potential link between binding kinetics and functional effects. All compounds fully displaced [^{3}H]LUF7482 in a dose-dependent manner at 15 °C (Fig. 2B), yielding K_i values summarized in Table 2. Consistent with K_D values obtained from kinetic and equilibrium binding assays, unlabeled LUF7482 exhibited nanomolar binding affinity (K_i = 22 nM). Overall, all compounds displayed high and comparable affinity to U2OS_hCCR2, with K_i values ranging from 10 to 53 nM. In our assay, LUF6980 showed the highest affinity (10 nM), whereas JNJ-27141491 displayed the lowest (53 nM).

3.3. Validation of the [^{3}H]LUF7482 competition association assay

With the k_{on} and k_{off} values of [^{3}H]LUF7482 obtained from association and dissociation assays, we further determined the k_{on} and k_{off} values of competing ligands via competition association assays based on the Motulsky-Mahan model [33]. The assay was first validated on U2OS_hCCR2 membranes in the absence (vehicle) or presence of unlabeled LUF7482 at 0.3-, 1-, and 3- fold IC_{50} concentrations (Fig. 3A, Table 1), competing with radiolabeled [^{3}H]LUF7482 at 15 °C. The k_{on} and k_{off} values of unlabeled LUF7482 in this standard competition association assay were determined as 2.1 × 10^7 M^{-1}·min^{-1} and 0.30 min^{-1}, respectively (Table 1), consistent with the on- and off- rates of radiolabeled [^{3}H]LUF7482 from association (k_{on} = 3.3 × 10^7 M^{-1}·min^{-1}, Fig. 1A) and dissociation assays (k_{off} = 0.12 min^{-1}, Fig. 1B). Correspondingly, the K_D of unlabeled LUF7482 derived from the

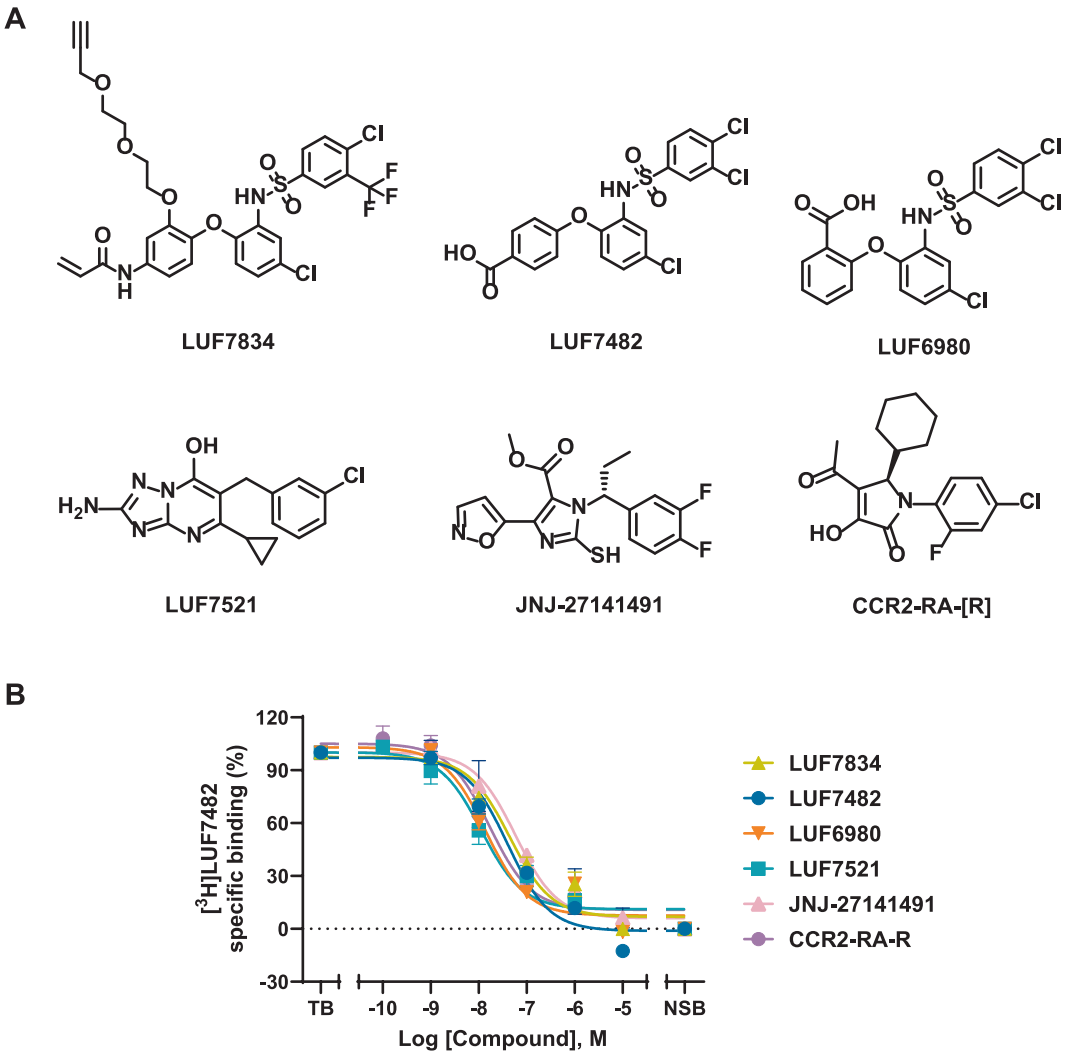

Fig. 2. [^{3}H] LUF7482 displacement by reference compounds on U2OS_hCCR2 membranes. (A) Chemical structures of the reference CCR2 intracellular antagonists: a covalent sulfonamide (LUF7834), sulfonamides (LUF7482, LUF6980), a triazolo-pyrimidinone (LUF7521), a 2-thioxoimidazoline (JNJ-27141491), and a pyrrolidinone (CCR2-RA-[*R*]). (B) Concentration-displacement curves of [^{3}H]LUF7482 by reference compounds (0.1 nM – 10 μM). Total binding (TB) was determined with DMSO control (1% DMSO), while non-specific binding (NSB) was determined with 10 μM LUF7721, and specific binding was calculated by subtracting NSB from TB. Data were fitted to a one-site competition model and are presented as mean ± SEM of at least three independent experiments, each performed in duplicate ($n = 3$: LUF7482 and JNJ-27141491; $n = 4$: LUF7834, LUF6980, LUF7521, and CCR2-RA-[*R*]). Parameters (pK_i, K_i) obtained from the [^{3}H]LUF7482 displacement assays are summarized in Table 2.

Table 2
Kinetic parameters of reference antagonists.

Compound	pK_i (K_i, nM)[b]	K_D (nM)[c]	k_{on} ($M^{-1}\cdot min^{-1}$)[d]	k_{off} (min^{-1})[e]	ET (min)[f]	RT (min)[g]
LUF7482	7.7 ± 0.1 (22)	17 ± 4	(1.8 ± 0.4) × 10^7	0.27 ± 0.05	0.07 ± 0.02	3.9 ± 0.6
LUF7834[a]	7.5 ± 0.1 (32)	7 ± 3	(4.1 ± 2.3) × 10^5	0.0018 ± 0.0002*	4.3 ± 1.6	576 ± 61*
LUF6980	8.0 ± 0.1 (10)	11 ± 4	(2.7 ± 2.3) × 10^8	1.8 ± 1.2	0.01 ± 0.01	1.3 ± 0.6
LUF7521	8.1 ± 0.3 (14)	24 ± 5	(2.1 ± 0.5) × 10^7	0.6 ± 0.2	0.05 ± 0.01	2.4 ± 0.7
JNJ-27141491	7.3 ± 0.0 (53)	38 ± 7	(2.9 ± 1.4) × 10^6	0.12 ± 0.07	1.0 ± 0.8	26 ± 18
CCR2-RA-[*R*]	7.8 ± 0.1 (16)	8 ± 2	(1.7 ± 0.1) × 10^6	0.014 ± 0.003*	0.59 ± 0.03***	93 ± 29

Values are presented as mean ± SEM from at least three independent experiments, each performed in duplicate. Kinetic parameters for all compounds were derived from simplified competition association assays performed at single concentration (1x IC_{50}). $n = 3$: LUF7834, LUF7521, JNJ-27141491, and CCR2-RA-[*R*]; $n = 4$: LUF7482 and LUF6980. Differences for reference compounds compared to LUF7482 were analyzed using Brown-Forsythe and Welch ANOVA with Dunnett's T3 multiple comparisons test: *$p < 0.033$; ***$p < 0.001$.

[a] Apparent equilibrium and kinetic values are presented for the covalent antagonist LUF7834.
[b] Binding affinity (pK_i, K_i) values from [^{3}H]LUF7482 displacement assays on U2OS_hCCR2 membranes at 15 °C (Fig. 2B).
[c] Kinetic K_D values, calculated as $K_D = k_{off} / k_{on}$.
[d] Association rate constant (k_{on}) of unlabeled compounds to U2OS_hCCR2 at 15 °C.
[e] Dissociation rate constant (k_{off}) of unlabeled compounds from U2OS_hCCR2 at 15 °C.
[f] Engagement time (ET) of compound at 1 μM, calculated as ET = 1 / (k_{on} × 10^{-6}).
[g] Residence time (RT) = 1 / k_{off}.

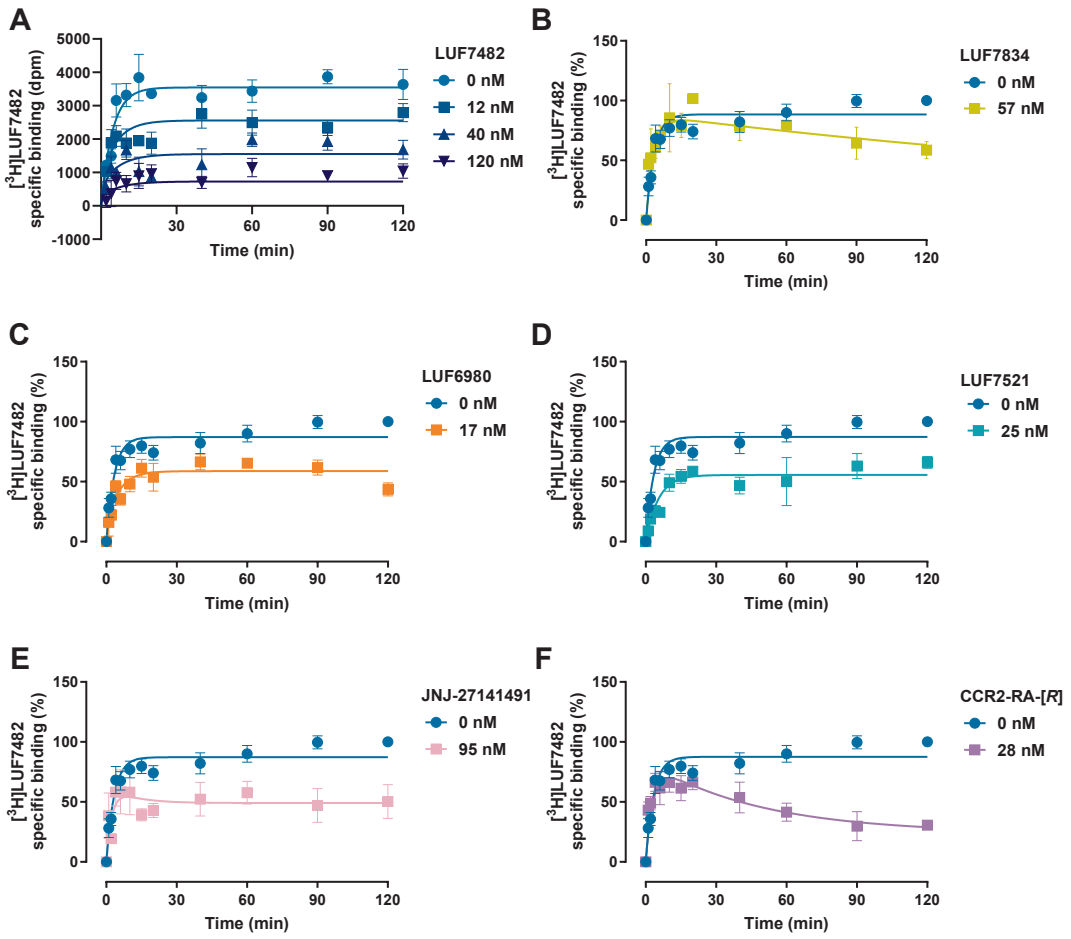

Fig. 3. [^{3}H] LUF7482 competition association assays with reference antagonists on U2OS_hCCR2 membranes at 15 °C. (A) Validation of [^{3}H]LUF7482 competition association assays (n = 4) with unlabeled LUF7482 at 0 nM (Vehicle), 12 nM (0.3x IC_{50}), 40 nM (1x IC_{50}) and 120 nM (3x IC_{50}). (B-F) Simplified competition association curves of [^{3}H]LUF7482 (~6.5 nM) in the absence (0 nM, blue, n = 7) or presence of competing reference antagonists at their 1x IC_{50} concentrations. (B) Covalent antagonist: LUF7834 (57 nM, grass green, n = 3); (C-F) Reversible antagonists: (C) LUF6980 (17 nM, orange, n = 4), (C) LUF7521 (25 nM, dark cyan, n = 3), JNJ-27141491 (95 nM, pink, n = 3), and CCR2-RA-[R] (28 nM, purple, n = 3). Data were fitted to the Motulsky-Mahan model and represent mean ± SEM of at least three independent experiments, each performed in duplicate. Kinetic parameters (K_D, k_{on}, k_{off}, RT) for LUF7482, derived from the validation curves (A), are summarized in the last row of Table 1. Kinetic parameters (K_D, k_{on}, k_{off}, ET, RT) for each competitive antagonist, derived from the competition association curves (B-F), are summarized in Table 2.

standard competition association assays (19 nM) closely matched the K_D of radiolabeled [^{3}H]LUF7482 from the classic association and dissociation assays (4 nM, Table 1), as well as the equilibrium K_D (10 nM) from the homologous displacement assay (Fig. 1C, Table 1). These K_D values were also comparable to the affinity of LUF7482 (K_i = 22 nM, Fig. 2B, Table 2) obtained from equilibrium displacement assays.

Taken together, these results demonstrated that the competition association assay can reliably determine k_{on} and k_{off} values of competing compounds on U2OS_hCCR2 membranes at 15 °C. Moreover, a simplified competition association assay, applying a single concentration of LUF7482 equal to 1x IC_{50} (40 nM), provided a robust experimental window (Fig. 3A) and kinetic parameters (LUF7482, Table 2) comparable to those obtained with standard three-concentration competition association assays (Table 1). These results demonstrate that a single concentration at 1x IC_{50} is sufficient for reliable determination of its binding kinetics. Hence, this set up was applied to subsequent reference compounds at a single concentration (1× IC_{50}) to increase assay throughput.

3.4. Kinetic characterization of reference CCR2 intracellular antagonists

Applying the validated competition association assay, we profiled the binding kinetics of five intracellular reference antagonists tested at a single IC_{50} concentration (Fig. 3B-F). The kinetic K_D values of these compounds, ranging from 7 to 38 nM, were in good agreement with their individual K_i values (10–53 nM, Table 2) obtained from radioligand displacement assays. Although all compounds displayed comparable nanomolar affinities, their kinetic behaviors varied substantially, with k_{on} values spanning from 4.1 × 10^5 to 2.7 × 10^8 M^{-1}·min^{-1}, and k_{off} values ranging from 0.0018 to 1.8 min^{-1} (Table 2).

The covalent positive control LUF7834 (Fig. 3B, Table 2), as expected, exhibited slow binding kinetics, with a markedly extended apparent residence time (RT) of 576 min, driven by a slow dissociation rate (apparent k_{off} = 0.0018 min^{-1}). These features resulted in a kinetic competition association curve (Fig. 3B) characterized by a peak in maximal binding within 10 min, which then declined slowly, well beyond the 120-min observation period. Of note, it also had a slow association rate (apparent k_{on} = 4.1 × 10^5 M^{-1}·min^{-1}, and an engagement time (ET) of 4.3 min at 1 μM, resulting in an apparent affinity that was comparable to the other antagonists.

Among the reversible antagonists, CCR2-RA-[R] exhibited the longest RT (93 min, Table 2), displaying a pronounced 'overshoot' in its competition association curve (Fig. 3F), peaking at submaximal binding at 10 min and gradually declining to half-maximal binding by 120 min (k_{on} = 1.7 × 10^6 M^{-1}·min^{-1}; k_{off} = 0.014 min^{-1}). JNJ-27141491 followed with the second-longest RT (26 min, Fig. 3E), showing an on-rate

comparable to CCR2-RA-[*R*], but a 9-fold higher k_{off} (k_{off} = 0.12 min^{-1}; k_{on} = 2.9 × 10^6 M^{-1}·min^{-1}). In contrast, LUF7482 (RT = 3.9 min, Fig. 3A), LUF6980 (RT = 1.3 min, Fig. 3C) and LUF7521 (RT = 2.4 min, Fig. 3D) had the shortest RTs (Table 2), with no 'overshoot' observed. Although LUF7482 and LUF6980 share the same sulfonamide core (Fig. 2A), LUF7482 displayed a 15-fold lower k_{on} and a seven-fold lower k_{off} than LUF6980, highlighting the influence of R-group substituents on kinetic behavior and pharmacological duration. Moreover, LUF6980 (k_{on} = 2.7 × 10^8 M^{-1}·min^{-1}; k_{off} = 1.8 min^{-1}) associated 158-fold faster and dissociated 128-fold faster than CCR2-RA-[*R*] (k_{on} = 1.7 × 10^6 M^{-1}·min^{-1}; k_{off} = 0.014 min^{-1}), suggesting a wide variation in kinetic profiles among these CCR2 antagonists.

Taken together, kinetic profiling revealed that the covalent antagonist LUF7834 exhibited a prolonged apparent RT, consistent with its irreversible mode of action. Among non-covalent antagonists, CCR2-RA-[*R*] showed the longest RT at CCR2, whereas LUF6980 had the shortest. These three compounds were therefore selected for further characterization in functional assays.

3.5. Functional characterization with GloSensor™ cAMP assay

To further investigate how antagonist binding kinetics relate to their functional behavior, GloSensor™ cAMP assays were performed in living U2OS_hCCR2 cells. Three intracellular antagonists were selected based on their distinct kinetic profiles: the shortest RT antagonist LUF6980 (RT = 1.3 min), the longest RT reversible antagonist CCR2-RA-[*R*] (RT = 93 min), and the covalent positive control LUF7834 (apparent RT = 576 min). To investigate a potential difference in their mode of antagonism, we compared their inhibition of CCL2-induced responses following a short (10 min) or a long (120 min) preincubation time. As such, CCL2-induced cAMP inhibition was measured in the absence (vehicle) or presence of an individual antagonist at fixed concentrations (30, 100, and 300 nM). After preincubation with or without antagonists, increasing concentrations of CCL2 (10 pM – 0.3 μM) were added and co-incubated for 90 min. CCL2-induced receptor activation resulted in a concentration-dependent reduction in forskolin-induced intracellular cAMP levels. Representative luminescence traces following CCL2 stimulation at a submaximal concentration (10 nM), in the absence (grey) or presence of LUF7834 (green), are shown in Fig. 4A-B. From these traces, the area under the curve (AUC) was calculated after CCL2 stimulation at increasing concentrations (10 pM – 0.3 μM) and fitted into concentration–response curves (Fig. 4C-H).

In absence of antagonist, increasing concentrations of CCL2 produced comparable cAMP inhibition following 10 min and 120 min preincubation, yielding identical EC_{50} values of 3 nM (Table 3). Preincubation with antagonists reduced CCL2-induced signaling, depending on compound, concentration, and preincubation time. In general, higher antagonist concentrations and longer preincubation times produced a greater rightward shift of the CCL2 response curves, reducing potency (EC_{50}) and, in some cases, maximal response (E_{max}), which is indicative of insurmountable antagonism.

The extent of these reductions varied among antagonists and showed a clear correlation with their RTs. Consistent with its short-RT, LUF6980 behaved as a competitive, surmountable antagonist after 10 min of preincubation (Fig. 4C) but became progressively insurmountable when preincubation was extended to 120 min (Fig. 4D). Accordingly, during short incubation, the E_{max} values of CCL2-induced cAMP responses were largely unaffected by LUF6980 across different concentrations, whereas a significantly E_{max} decrease was observed at 300 nM (73%, Table 3) following prolonged preincubation. Nevertheless, both 100 nM and 300 nM LUF6980 significantly reduced CCL2 potency irrespective of preincubation duration. Extending the preincubation time to 120 min did not produce any further shift in potency, even at the highest concentration, with comparable EC_{50} values between the two preincubation times (Table 3).

In contrast, the longest RT antagonist CCR2-RA-[*R*] exhibited clear insurmountable antagonism after preincubation for both 10 min (Fig. 4E) and 120 min (Fig. 4F) durations. Already after 10 min preincubation, the E_{max} values of CCL2-induced cAMP responses were significantly reduced with 300 nM CCR2-RA-[*R*] (59%, Table 3) compared to control, accompanied by a significant decrease in potency at both 100 nM (EC_{50} = 16 nM) and 300 nM (EC_{50} = 66 nM). Notably, this insurmountable effect became more pronounced with extended preincubation, as the E_{max} at 300 nM CCR2-RA-[*R*] significantly declined from 59% (10 min) to 35% (120 min preincubation), whereas responses at 30 nM and 100 nM remained largely unchanged (Table 3).

The covalent, and thus apparent longest-RT, antagonist LUF7834 displayed pronounced, time-dependent insurmountability. After only 10 min of preincubation, the E_{max} value was significantly reduced even at the lowest concentration of antagonist (56% at 30 nM) and dropped further at higher concentrations (37% and 15% at 100 nM and 300 nM, respectively), while potency remained consistent across concentrations (Fig. 4G, Table 3). This non-competitive, insurmountable behavior became more pronounced with prolonged preincubation (120 min, Fig. 4H), as only 30 nM LUF7834 nearly completely abolished CCL2-induced cAMP signaling (E_{max} = 2%, Table 3). Taken together, these findings support our hypothesis that the extent of functional insurmountable antagonism strongly correlates with the target binding kinetics of an allosteric antagonist.

Table 3
Functional characterization of LUF6980, CCR2-RA-[*R*], and LUF7834 in CCL2-induced GloSensor™ cAMP assays.

Compound	10 min Preincubation		120 min Preincubation	
	E_{max} (%)[a]	pEC_{50} ± SEM (EC_{50}, nM)[b]	E_{max} (%)[a]	pEC_{50} ± SEM (EC_{50}, nM)[b]
0 nM (CCL2)	100 ± 1	8.5 ± 0.1 (3)	100 ± 1	8.6 ± 0.1 (3)
+ **30 nM LUF6980**	98 ± 7	8.4 ± 0.1 (4)	100 ± 0	8.3 ± 0.1 (5)
+ **100 nM LUF6980**	102 ± 9	8.2 ± 0.1 (7)	105 ± 5	7.7 ± 0.2 (27) *
+ **300 nM LUF6980**	90 ± 7	7.6 ± 0.1 (26)**	73 ± 9*	7.7 ± 0.2 (24) *
+ **30 nM CCR2-RA-[*R*]**	98 ± 5	8.2 ± 0.1 (6)	95 ± 10	8.4 ± 0.1 (5)
+ **100 nM CCR2-RA-[*R*]**	88 ± 6	7.8 ± 0.1 (16)**	77 ± 8	8.0 ± 0.1 (11) *
+ **300 nM CCR2-RA-[*R*]**	59 ± 8*	7.2 ± 0.2 (66)*	35 ± 6*, +	7.3 ± 0.1 (50) ***
+ **30 nM LUF7834**	56 ± 6*	8.3 ± 0.1 (5)	2 ± 4**, ++	*N.A.*
+ **100 nM LUF7834**	37 ± 3**	8.4 ± 0.2 (5)	−1 ± 2***, ++	*N.A.*
+ **300 nM LUF7834**	15 ± 4**	8.9 ± 0.4 (2)	8 ± 5**	*N.A.*

Data represent the mean ± SEM of at least three independent experiments performed in duplicate. Potency (pEC_{50}, EC_{50}) and maximum responses (E_{max}) of CCL2 were measured in the absence (0 nM) or presence of representative antagonists (30, 100, and 300 nM), following either 10 min or 120 min preincubating with U2OS_hCCR2 cells. *N.A.*, not applicable.

Differences in potency or efficacy in the presence of antagonists (30, 100, and 300 nM) compared to the absence of antagonist (0 nM) were analyzed using Brown-Forsythe and Welch ANOVA with Dunnett's T3 multiple comparisons test: *$p < 0.033$; **$p < 0.002$; ***$p < 0.001$. Differences between preincubation durations (10 min vs. 120 min) were analyzed using Welch's *t*-test: $^{+}p < 0.033$; $^{++}p < 0.002$.

[a] The percentage of E_{max} represents the normalized luminescence response at 0.3 μM CCL2, derived from the concentration–response curves, with AUC values normalized to vehicle (0%, 0 nM CCL2) and E_{max} (100%, 0.3 μM CCL2) of control CCL2 curves in the absence of antagonist.

[b] Potency values (pEC_{50}, EC_{50}) of CCL2 responses were calculated by fitting area under the curve (AUC) values to the non-linear regression using 'log (agonist or inhibitor) vs. response (three parameters)'.

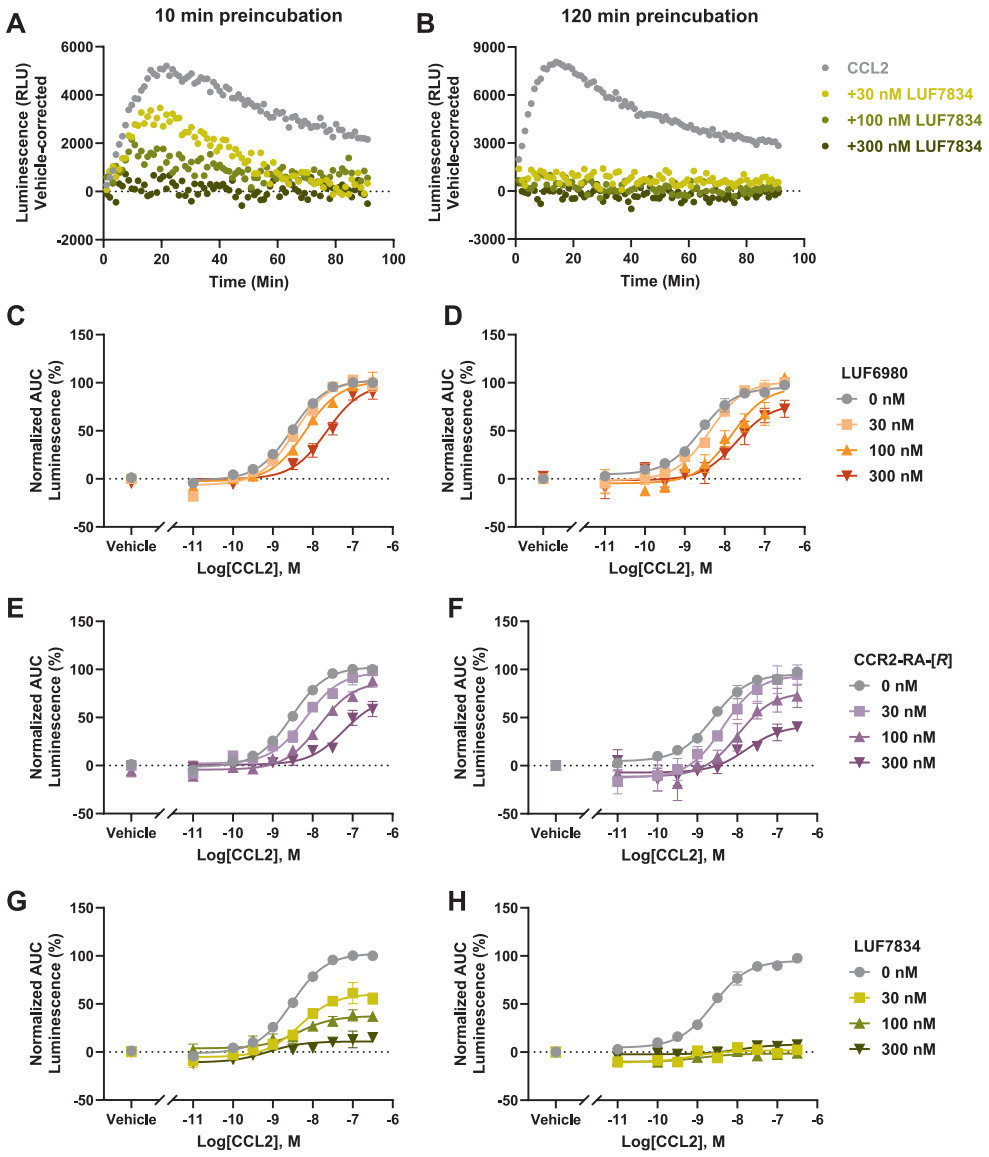

Fig. 4. Functional characterization of LUF6980, CCR2-RA-[*R*], and LUF7834 with CCL2-induced GloSensor™ cAMP assays in U2OS_hCCR2 cells. Cells were first stimulated with forskolin (1 μM), then preincubated with antagonists for 10 or 120 min (left vs. right panels), and subsequently induced with CCL2. Luminescence was monitored for 90 min following CCL2 addition. (A-B) Representative luminescence traces, expressed as relative light units (RLU), following CCL2 stimulation at a submaximal concentration (10 nM), after 10 min (A) or 120 min (B) preincubation with vehicle (grey), or increasing concentrations of LUF7834 (30, 100, and 300 nM; green gradient). Data are representative of three independent assays performed in duplicate. RLU responses were subsequently quantified by calculating the area under the curve (AUC) and fitting to nonlinear regression curves. (C-H) Concentration-response curves for CCL2 (10 pM – 0.3 μM), after preincubation with vehicle (0 nM, grey, $n = 10$ for 10 min and $n = 9$ for 120 min), or representative antagonists at 30, 100, and 300 nM: LUF6980 (orange gradient, $n = 4$ for 10 min and $n = 3$ for 120 min, C-D); CCR2-RA-[*R*] (purple gradient, $n = 3$, E-F); the covalent antagonist LUF7834 (green gradient, $n = 3$, G-H). Data are presented as mean ± SEM of at least three independent experiments performed in duplicate. Potency (pEC_{50}, EC_{50}) and efficacy (E_{max}) values derived from the concentration–response curves are summarized in Table 3.

4. Discussion

Binding kinetics has increasingly emerged as a critical determinant in early drug discovery, complementing traditional equilibrium parameters such as affinity. While affinity provides a static measure of ligand-receptor interactions, and is often insufficient to predict *in vivo* efficacy alone, kinetic parameters capture the dynamics of ligand-receptor engagement, thereby shaping both the magnitude and duration of drug pharmacodynamics [36]. Compounds with favorable kinetic profiles, particularly slow dissociation and thus an sustained target RT, often achieve enhanced *in vivo* efficacy at lower doses [11,36,37].

Due to the limited investigation of intracellular tracers, most kinetic studies have focused on orthosteric ligands for GPCRs [38,39]. In contrast to the binary complex for orthosteric antagonists, intracellular allosteric antagonists introduce an additional layer of kinetic complexity, as described by the allosteric ternary complex model involving both orthosteric and allosteric ligands [40]. Previous kinetic attempts for CCR2 intracellular allosteric radioligand were unsuccessful. Specifically, [^{3}H]CCR2-RA exhibited a monophasic association but biphasic dissociation, with k_{obs} of 0.09 min^{-1}, and two dissociation constants (k_{off1} = 0.24 min^{-1} and k_{off2} = 0.03 min^{-1} [24]). Similarly, kinetic characterization of [^{3}H]CCR2-RA-[*R*] revealed biphasic behaviors in both association and dissociation phases [27]. Due to these complex kinetic profiles, the Motulsky-Mahan model [33] could not be used (i.e. as a single k_{on}/k_1 and single k_{off}/k_2 needed), precluding their application for kinetic profiling of competing compounds.

Thus, in this study we introduced an allosteric radioligand [^{3}H]LUF7482, enabling direct kinetic characterization of intracellular allosteric CCR2 antagonists. In this setup, the allosteric antagonists directly compete with [^{3}H]LUF7482 at the same intracellular binding site, avoiding additional complications from allosteric cooperativity [41]. Because [^{3}H]LUF7482 displayed rapid association and dissociation at 25 °C, accurate determination of kinetic parameters was only possible at a reduced temperature of 15 °C. Similar temperature adjustments have been applied to other targets, e.g. adenosine A_{2A} receptor (A_{2A}R, [31]) and human equilibrative nucleoside transporter 1 (hENT$_1$, [42]), where kinetic assays were performed at temperatures as low as 5 °C [31] and 10 °C [42], respectively. The K_D and B_{max} of [^{3}H]LUF7482 at 15 °C were 10 nM and 6.3 pmol/mg, respectively, closely matching previously obtained parameters at 25 °C on HEK293T-CCR2 membranes (K_D = 6.5 nM, B_{max} = 10 pmol/mg [35]). Notably, the consistent K_D values obtained from both equilibrium and kinetic studies, along with the concordant k_{on} and k_{off} values of LUF7482 derived from both classical and competitive kinetic studies, validate the robustness of our kinetic assay.

Evaluation of structurally diverse intracellular reference compounds, as expected, revealed consistently high affinities for CCR2, comparable to previously published affinities tested at 25 °C on U2OS_CCR2 membranes. Specifically, in [^{3}H]CCR2-RA-[*R*] displacement assays, LUF7834 exhibited an apparent K_i value of 8 nM (compound 6c in [30]), while LUF7521 had a K_i value of 1.3 nM (compound 8 in [23]). In assays competing with racemic [^{3}H]CCR2-RA, LUF6980 (SD-24), CCR2-RA-[*R*], LUF7482 (compound 7 in [28]), and JNJ-27141491 displayed K_i values of 1 nM [26], 5 nM [24], 6 nM [28], and 12 nM [24], respectively. Notably, their K_i ranking: LUF6980 < LUF7521 < CCR2-RA-[R] < LUF7834 < JNJ-27171491, matches perfectly with that observed in this study at 15 °C (Table 2), demonstrating that while absolute values vary with temperature, relative affinities and trends are consistent.

Although these intracellular antagonists displayed comparable affinities, they exhibited pronounced diversity in their binding kinetic behavior. This observation reinforces the emerging concept that affinity alone does not predict target occupancy duration. For instance, despite comparable K_i and K_D values, the pyrrolone derivative CCR2-RA-[*R*] exhibited slower association and dissociation relative to the sulfonamide derivative LUF6980. In addition, the reversible antagonists LUF7482 and LUF6980, which share an identical sulfonamide core, displayed different kinetic profiles, highlighting the role of R-group substituents in modulating kinetic behavior and extending pharmacological duration, also at an allosteric site. Discrepancies between affinity and kinetics have been reported for numerous receptors, including adenosine A_1 receptor [43], glucagon-like peptide-1 receptor [44], metabotropic glutamate receptor 2 [45], and 5-hydroxytryptamine 7 receptor [46], as well as hENT$_1$, where a draflazine derivative showed ~10-fold slower association and ~100-fold slower dissociation than a dipyridamole analogue, despite similar nanomolar affinities [47].

The kinetics of some compounds investigated herein have also been studied previously, albeit in NanoBRET assays at room temperature, which can be performed in live cells [29]. For example, CCR2-RA-[*R*] exhibited a ~3.5 fold longer RT at 15 °C (93 min, Table 2) than its racemic mixture CCR2-RA at room temperature (27 min) in NanoBRET assays [29]. In contrast, the shortest-RT antagonist identified here, LUF6980, showed a nine-fold shorter RT at 15 °C (1.3 min, Table 2) than in NanoBRET assays at room temperature (12 min [29]). As these studies differ in temperature, assay format, and because the racemic mixture CCR2-RA differs with the pure enantiomer CCR2-RA-[*R*] used here, differences in kinetic behavior are expected. Nevertheless, the overall trends are consistent. CCR2-RA-[*R*] and its racemic mixture consistently displayed longer RTs than LUF6980 in both assays, supporting the robustness and reliability of our binding kinetic measurements.

Of note, this NanoBRET-based method has recently also been employed to study the kinetics of other intracellular antagonists at different chemokine receptors. In CCR7, the molecular tool Mz437 was characterized by rapid kinetics, resulting in a residence time of 4.5 min at room temperature [48], which is comparable to the RT of LUF7482 (3.9 min, Table 2) at 15 °C in this study. While in CCR9, a Vercirnon analogue displayed a long RT of 90 min when tested at a higher temperature of 37 °C [49], comparable to the RT of CCR2-RA-[*R*] (93 min, Table 2) in our study. However, although studying the binding kinetics of antagonists targeting the intracellular binding site of chemokine receptors is gaining attention, none of these studies have looked into how these kinetics influence functional outcomes.

Given the high local concentrations of endogenous chemokines (e.g. CCL2) under inflammatory or pathophysiological conditions, enhanced insurmountable antagonism is particularly advantageous for targeting chemokine receptors in chronic diseases like cancer or autoimmune disease [53]. Our functional studies revealed a strong correlation between the level of insurmountable antagonism and the kinetic profile of the selected ligands. Prolonged incubation (120 min) had little impact on the short-RT antagonist (LUF6980) but markedly enhanced the insurmountable behavior of long-RT compounds, particularly LUF7834. Such a link between binding kinetics and functional effects has been previously investigated for orthosteric antagonists targeting other GPCRs. For instance, a series of thiophene derivatives targeting the orthosteric site of the cannabinoid receptor 1, exhibited significant differences in residence time, which correlated with their insurmountable antagonism in both [^{35}S]GTPγS binding and β-arrestin recruitment assays [50]. A similar case has been observed at adenosine A_{2A} receptor, where triazolotriazine-derived antagonists displayed only minor differences in affinity but varied substantially in their residence times [51]. In this example, the selected long-RT antagonist exhibited insurmountable antagonism in a cAMP assay, whereas the functional effect of the shortest-RT antagonist was surmountable. A similar correlation between RT and insurmountable antagonism has been observed for angiotensin II type I receptor antagonists (Sartans) [52], contributing to their long-lasting antihypertensive effect *in vivo*.

Of note, all three selected ligands for the functional assays (LUF6980, CCR2-RA-[*R*], and LUF7834) displayed good consistency between membrane-based and live-cell assays, indicating adequate cellular permeability. LUF6980 exhibited functional potency in cell-based IP turnover assays (EC_{50} = 236 nM [26]) consistent with its low-nanomolar binding affinity (K_i = 5 nM [24]), while CCR2-RA-[*R*] displayed concordant binding (K_i = 5 nM [24]) and live-cell functional potencies in β-arrestin-2 recruitment (EC_{50} = 25 nM [24]) and cell-impedance assays (EC_{50} = 64 nM [24]). Although LUF7834 has not previously been evaluated in live-cell assays, our data suggest adequate permeability, as it achieved ~50% inhibition at 30 nM and near-complete inhibition at 300 nM after a 10 min preincubation in the GloSensor™ cAMP assay (Fig. 4G, Table 3), aligning well with its binding affinity (K_i = 32 nM, Table 2).

Beyond RT, association kinetics may also play a key role in achieving high target occupancy and influencing insurmountable antagonism. Faster association can enhance initial receptor occupancy, particularly before the system reaches equilibrium, and can prolong intracellular target engagement by promoting rebinding [13], where the drug re-associates with their target rather than diffusing away. This cycle of rapid rebinding and slow dissociation extends intracellular residence time and pharmacodynamic duration, as demonstrated by Gebre *et al.* [12] and Vauquelin *et al.* [13], highlighting the significance of association rates in drug design. For intracellular antagonists in particular, local ligand concentrations may remain higher than extracellular ligands, making rebinding a more significant factor.

In this case, association kinetics are particularly relevant when the shortest preincubation time of 10 min was used, as equilibrium may not have been reached for all antagonist concentrations. The ET of the slowest-associating compound, LUF7834 (ET = 4.3 min, Table 2) demonstrates that at 1 μM it can effectively engage the receptor within the 10-min preincubation period. However, substantially longer ETs are

required at lower concentrations (approximately 33- and 10-fold longer for 30 nM and 100 nM, respectively, according to ET $= 1/(k_{on} \times [L])$). Under these conditions, full receptor occupancy is not expected for 10 min preincubation. Consequently, due to signal amplification in the cAMP assays, a fraction of receptors likely remains available for agonist activation, resulting in residual agonist responses in the functional cAMP data (Fig. 4G), where 56% and 37% residual activity were observed at 30 and 100 nM LUF7834, respectively (Table 3). However, potential contributions of ligand rebinding, cannot be excluded. In contrast, for the fastest-associating compound, LUF6980, no insurmountable behavior was observed after 10 min preincubation, despite its allosteric binding mode. Given its short engagement time (ET = 0.01 min at 1 μM, Table 2), 10 min is sufficient for full receptor engagement even at the lowest concentration (30 nM). Therefore, its surmountable behavior is most likely driven by its very short RT, resulting in incomplete occupancy and residual agonist activity at both incubation times. Notable, the prolonged incubation period (120 min) allows all three antagonists to fully engage the receptor, thereby ruling out of a contribution of association rate to their insurmountable behaviors. Together, these data suggest that although RT is the primary driver for insurmountable antagonism under prolonged incubation times, ET may contribute to the initial insurmountable behavior of slowly associating antagonists before equilibrium is reached.

Fast-associating antagonists may be preferable when an immediate effect is desired, whereas slow-dissociating compounds can sustain efficacy in chronic diseases such as cancer or autoimmune disease [53]. When receptor RT exceeds the pharmacokinetic half-life, pharmacodynamic effects may persist beyond system clearance, potentially reducing dosing frequency and minimizing off-target toxicity [42,54]. As exemplified by $mGlu_2R$ positive allosteric modulators, the long-RT 7-Aryl-1,2,4-triazolo[4,3-a]pyridine derivative (referred to as compound 9 in [45]) shows extended duration of action *in vitro* (impedance-based morphology) and sustained inhibition of rapid eye movement *in vivo* compared with its short-RT analogue (compound 20 in [45]).

In this study, we established and validated a kinetic binding assay to characterize intracellular allosteric CCR2 antagonists. Despite their comparable high affinities, the reference compounds exhibited strikingly divergent kinetic behaviors, with residence times ranging from minutes to several hours. Functional outcomes further demonstrated that binding kinetics strongly correlated with their level of insurmountable antagonism, which further validates the predictive value of our competitive association assays for characterizing intracellular CCR2 antagonists. Collectively, these findings highlight the importance of incorporating kinetic profiling alongside affinity assessment in early drug discovery. Beyond CCR2, our approach provides a generalizable framework for studying the kinetic properties of intracellular ligands, and for designing compounds optimized not only for binding affinity but also for their binding kinetics to obtain an enhanced *in vivo* pharmacological efficacy.

CRediT authorship contribution statement

Yao Yao: Writing – original draft, Visualization, Validation, Methodology, Investigation, Formal analysis, Data curation. **Lisa S. den Hollander:** Methodology, Investigation. **Bente Bleijs:** Investigation, Formal analysis, Data curation. **Thomas Hartung:** Resources. **Uwe Grether:** Resources. **Natalia V. Ortiz Zacarías:** Writing – review & editing, Supervision, Project administration, Methodology, Conceptualization. **Laura H. Heitman:** Writing – review & editing, Supervision, Project administration, Methodology, Funding acquisition, Conceptualization.

Declaration of competing interest

The authors declare that they have no known competing financial interests or personal relationships that could have appeared to influence the work reported in this paper.

Acknowledgments

This publication is financed by the Chinese Scholarship Council (CSC) and Oncode Institute.

Data availability

Data will be made available on request.

References

[1] H. Raghu, et al., CCL2/CCR2, but not CCL5/CCR5, mediates monocyte recruitment, inflammation and cartilage destruction in osteoarthritis, Ann. Rheum. Dis. 76 (5) (2017) 914–922, https://doi.org/10.1136/annrheumdis-2016-210426.
[2] S. Abid, et al., CCR2/CCR5-mediated macrophage–smooth muscle cell crosstalk in pulmonary hypertension, Eur. Respir. J. 54 (4) (2019) 1802308, https://doi.org/10.1183/13993003.02308-2018.
[3] S. Pozzi, R. Satchi-Fainaro, The role of CCL2/CCR2 axis in cancer and inflammation: the next frontier in nanomedicine, Adv. Drug Deliv. Rev. 209 (2024) 115318, https://doi.org/10.1016/j.addr.2024.115318.
[4] B. Huang, et al., CCL2/CCR2 pathway mediates recruitment of myeloid suppressor cells to cancers, Cancer Lett. 252 (1) (2007) 86–92, https://doi.org/10.1016/j.canlet.2006.12.012.
[5] D. Guo, W. Zhu, H. Qiu, C-C motif chemokine ligand 2 and chemokine receptor 2 in cardiovascular and neural aging and aging-related diseases, Int. J. Mol. Sci. 25 (16) (2024) 8794, https://doi.org/10.3390/ijms25168794.
[6] H. Li, M. Wu, X. Zhao. Role of chemokine systems in cancer and inflammatory diseases. MedComm (Beijing). 3(2) (2022), doi: 10.1002/mco2.147.
[7] V. Ratziu, et al., Cenicriviroc treatment for adults with nonalcoholic steatohepatitis and fibrosis: final analysis of the phase 2b CENTAUR study, Hepatology 72 (3) (2020) 892–905, https://doi.org/10.1002/hep.31108.
[8] A. Junker, A.K. Kokornaczyk, A.K. Strunz, B. Wünsch. Selective and dual targeting of CCR2 and CCR5 receptors: a current overview, (2014), pp. 187–241. doi: 10.1007/7355_2014_40.
[9] D. Guo, L.H. Heitman, A.P. IJzerman, The role of target binding kinetics in drug discovery, ChemMedChem 10 (11) (2015) 1793–1796, https://doi.org/10.1002/cmdc.201500310.
[10] K.S.S. Lee, et al., Drug-target residence time affects in vivo target occupancy through multiple pathways, ACS Cent. Sci. 5 (9) (2019) 1614–1624, https://doi.org/10.1021/acscentsci.9b00770.
[11] S.K. Kordylewski, R. Bugno, S. Podlewska, Residence time in drug discovery: current insights and future perspectives, Pharmacol. Rep. 77 (4) (2025) 851–873, https://doi.org/10.1007/s43440-025-00748-z.
[12] S.T. Gebre, S.A. Cameron, L. Li, Y.S. Babu, V.L. Schramm, Intracellular rebinding of transition-state analogues provides extended in vivo inhibition lifetimes on human purine nucleoside phosphorylase, J. Biol. Chem. 292 (38) (2017) 15907–15915, https://doi.org/10.1074/jbc.M117.801779.
[13] G. Vauquelin. Rebinding: or why drugs may act longer in vivo than expected from their in vitro target residence time. (2010). doi: 10.1517/17460441.2010.512037.
[14] N. Yin, J. Pei, L. Lai, A comprehensive analysis of the influence of drug binding kinetics on drug action at molecular and systems levels, Mol. Biosyst. 9 (6) (2013) 1381, https://doi.org/10.1039/c3mb25471b.
[15] H. Lu, et al., Slow-onset inhibition of the FabI enoyl reductase from francisella tularensis: residence time and in vivo activity, ACS Chem. Biol. 4 (3) (2009) 221–231, https://doi.org/10.1021/cb800306y.
[16] H. Liu, H. Zhang, A.P. IJzerman, D. Guo, The translational value of ligand-receptor binding kinetics in drug discovery, Br. J. Pharmacol. 181 (21) (2024) 4117–4129, https://doi.org/10.1111/bph.16241.
[17] H. Zhang, et al., Long residence time at the vasopressin V2 receptor translates into superior inhibitory effects in ex vivo and in vivo models of autosomal dominant polycystic kidney disease, J. Med. Chem. 65 (11) (2022) 7717–7728, https://doi.org/10.1021/acs.jmedchem.2c00011.
[18] D.J. Dairaghi, et al., Pharmacokinetic and pharmacodynamic evaluation of the novel CCR1 antagonist CCX354 in healthy human subjects: Implications for selection of clinical dose, Clin. Pharmacol. Ther. 89 (5) (2011) 726–734, https://doi.org/10.1038/clpt.2011.33.
[19] T.J. Schall, A.E.I. Proudfoot, Overcoming hurdles in developing successful drugs targeting chemokine receptors, Nat. Rev. Immunol. 11 (5) (2011) 355–363, https://doi.org/10.1038/nri2972.
[20] I. Bot, et al., A novel CCR2 antagonist inhibits atherogenesis in apoE deficient mice by achieving high receptor occupancy. Sci. Rep. 7(1) (2017), doi: 10.1038/s41598-017-00104-z.
[21] L.M. Slosky, et al., β-arrestin-biased allosteric modulator of NTSR1 selectively attenuates addictive behaviors, Cell 181 (6) (2020) 1364–1379.e14, https://doi.org/10.1016/j.cell.2020.04.053.
[22] J.S. Smith, R.J. Lefkowitz, S. Rajagopal, Biased signalling: from simple switches to allosteric microprocessors, Nat. Rev. Drug Discov. 17 (4) (2018) 243–260, https://doi.org/10.1038/nrd.2017.229.
[23] N.V. Ortiz Zacarías, et al., Synthesis and Pharmacological evaluation of triazolopyrimidinone derivatives as noncompetitive, intracellular antagonists for

CC chemokine receptors 2 and 5, J. Med. Chem. 62 (24) (2019) 11035–11053, https://doi.org/10.1021/acs.jmedchem.9b00742.
[24] A.J.M. Zweemer, et al., Multiple binding sites for small-molecule antagonists at the CC chemokine receptor 2, Mol. Pharmacol. 84 (4) (2013) 551–561, https://doi.org/10.1124/mol.113.086850.
[25] Y. Zheng, et al., Structure of CC chemokine receptor 2 with orthosteric and allosteric antagonists, Nature 540 (7633) (2016) 458–461, https://doi.org/10.1038/nature20605.
[26] A.J.M. Zweemer, et al., Discovery and mapping of an intracellular antagonist binding site at the chemokine receptor CCR2, Mol. Pharmacol. 86 (4) (2014) 358–368, https://doi.org/10.1124/mol.114.093328.
[27] N.V. Ortiz Zacarías, et al., Pyrrolone derivatives as intracellular allosteric modulators for chemokine receptors: selective and dual-targeting inhibitors of CC chemokine receptors 1 and 2, J. Med. Chem. 61 (20) (2018) 9146–9161, https://doi.org/10.1021/acs.jmedchem.8b00605.
[28] N.V. Ortiz Zacarías, et al., Design and characterization of an intracellular covalent ligand for CC chemokine receptor 2, J. Med. Chem. 64 (5) (2021) 2608–2621, https://doi.org/10.1021/acs.jmedchem.0c01137.
[29] L. Toy, M.E. Huber, M.F. Schmidt, D. Weikert, M. Schiedel, Fluorescent ligands targeting the intracellular allosteric binding site of the chemokine receptor CCR2, ACS Chem. Biol. 17 (8) (2022) 2142–2152, https://doi.org/10.1021/acschembio.2c00263.
[30] L.S. den Hollander, et al., Labeling of CC chemokine receptor 2 with a versatile intracellular allosteric probe, ACS Chem. Biol. 19 (9) (2024) 2070–2080, https://doi.org/10.1021/acschembio.4c00439.
[31] D. Guo, T. Mulder-Krieger, A.P. IJzerman, L.H. Heitman, Functional efficacy of adenosine a 2A receptor agonists is positively correlated to their receptor residence time, Br. J. Pharmacol. 166 (6) (2012) 1846–1859, https://doi.org/10.1111/j.1476-5381.2012.01897.x.
[32] Y. Cheng, W.H. Prusoff, Relationship between the inhibition constant (K1) and the concentration of inhibitor which causes 50 per cent inhibition (I50) of an enzymatic reaction, Biochem. Pharmacol. 22 (23) (1973) 3099–3108, https://doi.org/10.1016/0006-2952(73)90196-2.
[33] H.J. Motulsky, L.C. Mahan, The kinetics of competitive radioligand binding predicted by the law of mass action, Mol. Pharmacol. 25 (1) (1984) 1–9.
[34] X. Li, et al., Structural basis of selective cannabinoid CB2 receptor activation. Nat. Commun., 14(1) (2023), doi: 10.1038/s41467-023-37112-9.
[35] L.S. den Hollander, et al., Impact of cancer-associated mutations in CC chemokine receptor 2 on receptor function and antagonism. Biochem. Pharmacol., 208 (2023), doi: 10.1016/j.bcp.2022.115399.
[36] K.E. Knockenhauer, R.A. Copeland. The importance of binding kinetics and drug–target residence time in pharmacology. (2024), John Wiley and Sons Inc. doi: 10.1111/bph.16104.
[37] D. Guo, J.M. Hillger, A.P. Ijzerman, L.H. Heitman, Drug-target residence time-a case for G protein-coupled receptors, Med. Res. Rev. 34 (4) (2014) 856–892, https://doi.org/10.1002/med.21307.
[38] M. Vilums, et al., Evaluation of (4-arylpiperidin-1-yl)cyclopentanecarboxamides as high-affinity and long-residence-time antagonists for the CCR2 receptor, ChemMedChem 10 (7) (2015) 1249–1258, https://doi.org/10.1002/cmdc.201500058.
[39] D.C. Swinney, et al., A study of the molecular mechanism of binding kinetics and long residence times of human CCR5 receptor small molecule allosteric ligands, Br. J. Pharmacol. 171 (14) (2014) 3364–3375, https://doi.org/10.1111/bph.12683.
[40] Ó. Díaz, V. Martín, P. Renault, D. Romero, A. Guillamon, J. Giraldo, Allosteric binding cooperativity in a kinetic context. (2023), Elsevier Ltd. doi: 10.1016/j.drudis.2022.103441.
[41] J.R. Lane, L.T. May, R.G. Parton, P.M. Sexton, A. Christopoulos, Akinetic view of GPCR allostery and biased agonism. (2017), Nature Publishing Group. doi: 10.1038/nchembio.2431.
[42] A. Vlachodimou, et al., Kinetic profiling of novel spirobenzo-oxazinepiperidinone derivatives as equilibrative nucleoside transporter 1 inhibitors, Purinergic Signal 20 (2) (2024) 193–205, https://doi.org/10.1007/s11302-023-09948-9.
[43] Y. Yun, et al., Long residence time adenosine A1 receptor agonists produce sustained wash-resistant antilipolytic effect in rat adipocytes, Biochem. Pharmacol. 164 (2019) 45–52, https://doi.org/10.1016/j.bcp.2019.03.032.
[44] P. Zhao, T.T. Truong, J. Merlin, P.M. Sexton, D. Wootten, Implications of ligand-receptor binding kinetics on GLP-1R signalling, Biochem. Pharmacol. 199 (2022), https://doi.org/10.1016/j.bcp.2022.114985.
[45] M.L.J. Doornbos, et al., Discovery and kinetic profiling of 7-Aryl-1,2,4-triazolo[4,3-a]pyridines: positive allosteric modulators of the metabotropic glutamate receptor 2, J. Med. Chem. 60 (15) (2017) 6704–6720, https://doi.org/10.1021/acs.jmedchem.7b00669.
[46] E. Penna, et al., In Vitro and in silico analysis of the residence time of serotonin 5-HT7 receptor ligands with arylpiperazine structure: a structure-kinetics relationship study, ACS Chem. Neurosci. 13 (4) (2022) 497–509, https://doi.org/10.1021/acschemneuro.1c00710.
[47] A. Vlachodimou, K. Konstantinopoulou, A.P. IJzerman, L.H. Heitman, Affinity, binding kinetics and functional characterization of draflazine analogues for human equilibrative nucleoside transporter 1 (SLC29A1). Biochem. Pharmacol. 172 (2020), doi: 10.1016/j.bcp.2019.113747.
[48] S.L. Wurnig, et al., A fluorescent probe enables the discovery of improved antagonists targeting the intracellular allosteric site of the chemokine receptor CCR7, J. Med. Chem. 68 (4) (2025) 4308–4333, https://doi.org/10.1021/acs.jmedchem.4c02102.
[49] M.E. Huber, et al., A chemical biology toolbox targeting the intracellular binding site of CCR9: fluorescent ligands, new drug leads and PROTACs, Angew. Chem. Int. Ed. Engl. 61 (12) (2022) e202116782, https://doi.org/10.1002/anie.202116782.
[50] L. Xia, et al., Kinetics of human cannabinoid 1 (CB1) receptor antagonists: Structure-kinetics relationships (SKR) and implications for insurmountable antagonism, Biochem. Pharmacol. 151 (2018) 166–179, https://doi.org/10.1016/j.bcp.2017.10.014.
[51] D. Guo, et al., Binding kinetics of ZM241385 derivatives at the human adenosine A2A receptor, ChemMedChem 9 (4) (2014) 752–761, https://doi.org/10.1002/cmdc.201300474.
[52] I. Van Liefde, G. Vauquelin, Sartan-AT1 receptor interactions: In vitro evidence for insurmountable antagonism and inverse agonism. (2009), doi: 10.1016/j.mce.2008.06.006.
[53] P.J. Tummino, R.A. Copeland, Residence time of receptor - ligand complexes and its effect on biological function, (2008). doi: 10.1021/bi8002023.
[54] R.A. Copeland, The drug-target residence time model: a 10-year retrospective, Nat. Rev. Drug Discov. 15 (2) (2016) 87–95, https://doi.org/10.1038/nrd.2015.18.